# SPECTRAL DOMAIN ANALYSIS OF RESONANT CHARACTERISTICS AND RADIATION PATTERNS OF A CIRCULAR DISC AND AN ANNULAR RING MICROSTRIP ANTENNA ON UNIAXIAL SUBSTRATE

## A. Motevasselian[*]

Lab of Electromagnetic Engineering, Department of Electrical Engineering, Royal Institute of Technology (KTH), Teknikringen 33, 10044 Stockholm, Sweden

**Abstract**—A full-wave analysis for determining the resonant frequency, quality factor and far-zone radiation patterns of a circular disk and annular ring microstrip patches, printed on a uniaxial anisotropic substrate is presented. Green's functions of the structure are determined in Hankel transform domain (HTD) using Hertz potential vectors. Galerkin's method, together with parsval's relation in Hankel transform domain is then applied to compute the resonant frequency and quality factor. The far-zone radiation patterns are expressed in terms of Hankel transforms of the tangential fields on the substrate. Wave equation is solved in cylindrical coordinates for the structure to estimate the basis function. The numerical results show that there are substantial deviations in calculated resonant frequency and quality factor when substrate dielectric anisotropy is considered. Furthermore, significant variations are seen in the radiation patterns of the structures due to substrate anisotropy. The variations of resonant frequency, quality factor and radiation patterns of the structure, with respect to anisotropy ratio of the substrate, for several values of substrate thickness and patch radius are presented.

## 1. INTRODUCTION

Some substrate materials used for integrated microwave circuits or printed antennas exhibit dielectric anisotropy. This phenomenon occurs either naturally in the material or is introduced during the manufacturing process. In addition, anisotropic substrates have become popular in the design of microwave integrated circuit components and microstrip antennas [1–8]. Uniaxial substrates have drawn more attention due to their availability in materials such as sapphire, boron nitride and E-10 ceramic-impregnated Teflon. Previous studies of anisotropic materials used in microwave devices indicate that the effects of anisotropy on the performance of such structures particularly in high frequencies cannot be ignored [1, 5, 6]. Furthermore, it has been shown that the performance of directional couplers can be improved by using the anisotropic substrates to equalize the even and odd mode phase velocities [2]. Therefore, many investigations are examining the effects of substrate anisotropy in microwave components performance.

Circular microstrip patch resonators can be used either as radiating antennas or as oscillators and filters in microwave integrated circuits (MIC's) [9]. In some applications such as arrays, circular geometry of the patch offers certain advantages over other configurations. The experimental results have shown that circular microstrip elements could be easily modified to produce a range of impedances, radiation patterns and frequencies of operation [10]. The studies on circular patch microstrip antennas with anisotropic substrate are in limited number [11–14].

Annular ring microstrip antennas, because of their flexibility for producing dual frequency treatment [16] and advantages for using in medical applications [15] are interesting to many researchers. This type of printed antenna can have a broader bandwidth than other shape of patch antenna by a proper choice of dimensions and the mode of operation. Because of these interests several studies are fasten to annular ring patch antennas [15–18]. Furthermore, ring resonators have found applications in circulators, hybrid junction filters and other microwave devices [19]. Several articles on ring patches on uniaxial substrates has been recently published [20–22].

In this study, HTD analysis is performed for the wave equation using Hertz potential vectors. Galerkin's method is then applied to eigenvalue problem for determining resonant frequency and quality factor in terms of structure dimensions and anisotropy ratio of the substrate. Angular spectrum of the aperture field and saddle point technique is used to find radiation patterns of each structure. The

results indicate that proper selection of anisotropy ratio could lead to wider band-width, smaller resonant frequency and greater antenna directivity.

## 2. FORMULATIONS OF THE PROBLEM

The geometry of the studied structures are shown in Fig. 1. The substrates are considered to be a uniaxial medium with permittivity tensor:

$$[\varepsilon] = \begin{bmatrix} \varepsilon_{xx} = \varepsilon_2 & 0 & 0 \\ 0 & \varepsilon_{yy} = \varepsilon_2 & 0 \\ 0 & 0 & \varepsilon_{zz} = \varepsilon_1 \end{bmatrix} \tag{1}$$

Magnetic and electric Hertz potential vectors are defined by the following equations respectively [23]

$$\mathbf{E} = -j\omega\mu_0 \nabla \times \mathbf{\Pi}_h \tag{2}$$

$$\mathbf{H} = j\omega\varepsilon_0 \nabla \times \mathbf{\Pi}_e \tag{3}$$

Since all field components can be represented in terms of axial component of Hertz vectors, we choose

$$\mathbf{\Pi}_h = \Pi_h \hat{\mathbf{a}}_z \tag{4}$$

$$\mathbf{\Pi}_e = \Pi_e \hat{\mathbf{a}}_z \tag{5}$$



(a)



(b)
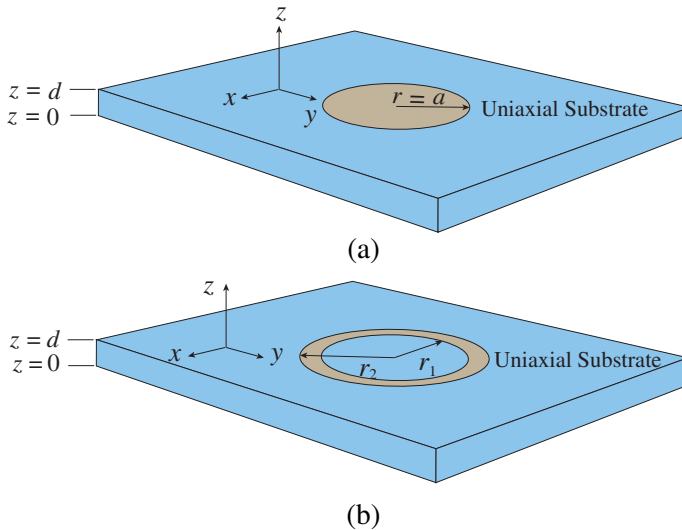
**Figure 1.** (a) Circular disk. (b) Annular ring microstrip antenna on uniaxial substrate.

Then all ordinary and extraordinary field components could be derived from

$$\mathbf{H} = -j\omega\varepsilon_0\nabla \times \mathbf{\Pi}_e + \nabla \times \nabla \times \mathbf{\Pi}_h \tag{6}$$

$$\mathbf{E} = \omega^2\mu_0\varepsilon_0\mathbf{\Pi}_e + \frac{\varepsilon_0}{\varepsilon_2}\nabla(\nabla.\mathbf{\Pi}_e) - j\omega\mu_0\nabla \times \mathbf{\Pi}_h. \tag{7}$$

where $\mathbf{\Pi}_e$ and $\mathbf{\Pi}_h$ are the solutions of the propagation equations of ordinary and extra ordinary waves

$$\nabla^2\mathbf{\Pi}_h + \omega^2\mu_0\varepsilon_2\mathbf{\Pi}_h = 0 \tag{8}$$

$$\nabla^2\mathbf{\Pi}_e + \omega^2\mu_0\varepsilon_1\mathbf{\Pi}_e + \frac{\varepsilon_1 - \varepsilon_2}{\varepsilon_2}\frac{\partial^2\mathbf{\Pi}_e}{\partial z^2} = 0 \tag{9}$$

Hankel transform pairs that are useful in a wide range of physical problems with an axial symmetry are represented in cylindrical coordinates as

$$\tilde{f}_n(\alpha) = \int_0^\infty f(\rho)J_n(\alpha\rho)\rho d\rho \tag{10}$$

$$f_n(\rho) = \int_0^\infty \tilde{f}(\alpha)J_n(\alpha\rho)\alpha d\alpha \tag{11}$$

Using this transform we have

$$\left(\frac{\partial^2}{\partial\rho^2} + \frac{1}{\rho}\frac{\partial}{\partial\rho} - \frac{n^2}{\rho^2}\right)f(\rho)\underset{\longleftrightarrow}{HT} - \alpha^2\tilde{f}_n(\alpha) \tag{12}$$

The propagation equations are now applied to the structures shown in Fig. 1. Using separation of variables technique and considering the periodicity of the structure with respect to angular variations, the Hertz vectors can be expressed in the form of

$$\Pi(\rho, \phi, z) = \Pi(\rho, z)e^{jn\phi} \tag{13}$$

Then we will have

$$\nabla^2\left(\Pi(\rho, z)e^{jn\phi}\right) = \Pi(\rho, z)e^{jn\phi}$$

$$= \left[\frac{\partial^2}{\partial\rho^2} + \frac{1}{\rho}\frac{\partial}{\partial\rho} + \frac{1}{\rho^2}\frac{\partial^2}{\partial\phi^2} + \frac{\partial^2}{\partial z^2}\right]\Pi(\rho, z)e^{jn\phi}$$

$$= e^{jn\phi}\left[\underbrace{\left(\frac{\partial^2}{\partial\rho^2} + \frac{1}{\rho}\frac{\partial}{\partial\rho} - \frac{n^2}{\rho^2}\right)}_{\text{equal to } -\alpha^2 \text{in HTD}}\Pi(\rho, z) + \frac{\partial^2\Pi(\rho, z)}{\partial z^2}\right] \tag{14}$$

Thus (5) and (6) in HTD have a simpler form of

$$\frac{\partial^2 \tilde{\Pi}_h(\alpha, z)}{\partial z^2} + \gamma_h^2 \tilde{\Pi}_h(\alpha, z) \tag{15}$$

$$\gamma_h^2 = (\omega^2 \mu_0 \varepsilon_2 - \alpha^2) \tag{16}$$

and

$$\frac{\partial^2 \tilde{\Pi}_e(\alpha, z)}{\partial z^2} + \gamma_e^2 \tilde{\Pi}_e(\alpha, z) \tag{17}$$

$$\gamma_e^2 = \frac{\varepsilon_2}{\varepsilon_1} (\omega^2 \mu_0 \varepsilon_1 - \alpha^2) \tag{18}$$

where $\gamma_h$ and $\gamma_e$ are the propagation constants along $z$-direction in HTD.

The solutions of (15) and (17) are:

In the uniaxial substrate region $0 < z < d$

$$\tilde{\Pi}_{h1}(\alpha, z) = A_{h1}(\alpha) \sin \gamma_{h1} z \tag{19}$$

$$\tilde{\Pi}_{e1}(\alpha, z) = B_{e1}(\alpha) \cos \gamma_{e1} z \tag{20}$$

where $\gamma_{h1}^2 = (\omega^2 \mu_0 \varepsilon_2 - \alpha^2)$ and $\gamma_{e1}^2 = \frac{\varepsilon_2}{\varepsilon_1} (\omega^2 \mu_0 \varepsilon_1 - \alpha^2)$; and in the substrate region $d < z$

$$\tilde{\Pi}_{h0}(\alpha, z) = A_{h0}(\alpha) e^{-j\gamma_{h0}(z-d)} \tag{21}$$

$$\tilde{\Pi}_{e0}(\alpha, z) = B_{e0}(\alpha) e^{-j\gamma_{e0}(z-d)} \tag{22}$$

where $\gamma_{h0}^2 = \gamma_{e0}^2 = (\omega^2 \mu_0 \varepsilon_0 - \alpha^2)$.

The total fields are obtained from (6) and (7) by taking inverse Hankel transform of (19)–(22). As an example the electric field components in the substrate region are

$$E_\rho = e^{jn\phi} \int_0^\infty -\frac{1}{\varepsilon_2} B_{e1} \gamma_{e1} \varepsilon_0 \sin(\gamma_{e1} z) \left[ \mp \alpha J_{n\pm1}(\alpha\rho) \pm \frac{n}{\rho} J_n(\alpha\rho) \right] \alpha d\alpha$$

$$+ e^{jn\phi} \int_0^\infty \omega \mu_0 \frac{n}{\rho} A_{h1} \sin(\gamma_{h1} z) J_n(\alpha\rho) \alpha d\alpha \tag{23}$$

$$E_\phi = e^{jn\phi} \int_0^\infty -\frac{1}{\varepsilon_2} \frac{jn}{\rho} B_{e1} \gamma_{e1} \varepsilon_0 \sin(\gamma_{e1} z) J_n(\alpha\rho) \alpha d\alpha$$

$$+ e^{jn\phi} \int_0^\infty j\omega \mu_0 A_{h1} \sin(\gamma_{h1} z) \left[ \mp \alpha J_{n\pm1}(\alpha\rho) \pm \frac{n}{\rho} J_n(\alpha\rho) \right] \alpha d\alpha \tag{24}$$

In these expressions, Bessel functions of different orders appear. Transformations become much easier if only single orders Bessel function are handled. Thus, tangential field components are arranged in a linear combination form [24]

$$F_{(\pm)} = F_\rho \pm j F_\phi \tag{25}$$

The resulting expressions in the uniaxial substrate medium and in air are:

In the uniaxial substrate region:

$$E_{1(\pm)} = e^{jn\phi} \int_0^\infty \pm \frac{1}{\varepsilon_2} B_{e1} \gamma_{e1} \alpha \varepsilon_0 \sin(\gamma_{e1} z) J_{n\pm1}(\alpha\rho) \alpha d\alpha$$

$$+ e^{jn\phi} \int_0^\infty \omega \mu_0 A_{h1} \alpha \sin(\gamma_{h1} z) J_{n\pm1}(\alpha\rho) \alpha d\alpha \tag{26}$$

$$H_{1(\pm)} = e^{jn\phi} \int_0^\infty -B_{e1} \omega \varepsilon_0 \alpha \cos(\gamma_{e1} z) J_{n\pm1}(\alpha\rho) \alpha d\alpha$$

$$\mp e^{jn\phi} \int_0^\infty A_{h1} \gamma_{h1} \alpha \cos(\gamma_{h1} z) J_{n\pm1}(\alpha\rho) \alpha d\alpha \tag{27}$$

In the free space region:

$$E_{0(\pm)} = e^{jn\phi} \int_0^\infty \pm j B_{e0} \gamma_{e0} \alpha e^{j\gamma_{e0}(z-d)} J_{n\pm1}(\alpha\rho) \alpha d\alpha$$

$$+ e^{jn\phi} \int_0^\infty \omega \mu_0 A_{h0} \alpha e^{-j\gamma_{h0}(z-d)} J_{n\pm1}(\alpha\rho) \alpha d\alpha \tag{28}$$

$$H_{0(\pm)} = e^{jn\phi} \int_0^\infty -B_{e0} \omega \varepsilon_0 \alpha e^{j\gamma_{e0}(z-d)} J_{n\pm1}(\alpha\rho) \alpha d\alpha$$

$$\mp e^{jn\phi} \int_0^\infty j A_{h0} \gamma_{h0} \alpha e^{j\gamma_{h0}(z-d)} J_{n\pm1}(\alpha\rho) \alpha d\alpha \tag{29}$$

The following boundary conditions at the interface of two regions are applied to eliminate the constant coefficients:

$$\tilde{E}_{1(\pm)} \mid_{z=d} = \tilde{E}_{0(\pm)} \mid_{z=d} \tag{30}$$

$$\pm j \left( \tilde{H}_{0(\pm)} - \tilde{H}_{0(\pm)} \right) \mid_{z=d} = \tilde{K}_{(\pm)} \tag{31}$$

where $K$ is the patch surface current density. Substituting the integrands of (26)–(29) which indicate the Hankel transform of the total field, into (30) and (31), yields the HTD relations between patch current density and tangential electric field at $z = d$ surface in matrix form yields

$$\begin{bmatrix} \tilde{K}_{(+)}(\alpha) \\ \tilde{K}_{(-)}(\alpha) \end{bmatrix} = \begin{bmatrix} Y_{++}(\alpha) & Y_{+-}(\alpha) \\ Y_{-+}(\alpha) & Y_{--}(\alpha) \end{bmatrix} \begin{bmatrix} \tilde{E}_{(+)}(\alpha) \\ \tilde{E}_{(-)}(\alpha) \end{bmatrix} \tag{32}$$

where

$$Y_{++}(\alpha) = Y_{--}(\alpha) = -\omega \varepsilon_0 \frac{1}{2\gamma_{e0}} - \gamma_{h0} \frac{1}{2\omega\mu_0} + j\omega\varepsilon_2 \frac{1}{2\gamma_{e1}} \cot(\gamma_{e1} d)$$

$$+ j\gamma_{h1} \frac{1}{2\omega\mu_0} \cot(\gamma_{h1} d) \tag{33}$$

$$Y_{++}(\alpha) = Y_{--}(\alpha) = \omega\varepsilon_0 \frac{1}{2\gamma_{e0}} - \gamma_{h0}\frac{1}{2\omega\mu_0} - j\omega\varepsilon_2\frac{1}{2\gamma_{e1}}\cot(\gamma_{e1}d)$$

$$+j\gamma_{h1}\frac{1}{2\omega\mu_0}\cot(\gamma_{h1}d) \tag{34}$$

Inverting (32), the impedance matrix is obtained as follows:

$$\begin{bmatrix} \tilde{E}_{(+)}(\alpha) \\ \tilde{E}_{(-)}(\alpha) \end{bmatrix} = \begin{bmatrix} Z_{++}(\alpha) & Z_{+-}(\alpha) \\ Z_{-+}(\alpha) & Z_{--}(\alpha) \end{bmatrix} \begin{bmatrix} \tilde{K}_{(+)}(\alpha) \\ \tilde{K}_{(-)}(\alpha) \end{bmatrix} \tag{35}$$

The impedance or admittance matrices given above are Green's function in the HTD of the structure.

## 3. GALERKIN'S METHOD AND CHARACTERISTIC EQUATIONS FOR EIGENVALUES

Up to this point, a closed form analytical solution is formulated. We now apply Galerkin's method to find the eigenvalues of (35). The unknown patch current density are expanded in linear combination of known basis functions as

$$K_{(\pm)}(\rho, \phi) = \sum_{n=-\infty}^{\infty} e^{jn\phi} \sum_{m=1}^{M} C_{m(\pm)}(n)K_{sm(\pm)}(\rho) \tag{36}$$

Equation (36) is written in HTD as

$$\tilde{K}_{(\pm)}(\alpha) = \sum_{m=1}^{M} C_{m(\pm)}\tilde{K}_{sm(\pm)}(\alpha) \tag{37}$$

Parseval's relation for HTD indicates that

$$\int_0^\infty f_1(\rho)f_2(\rho)\rho d\rho = \int_0^\infty \tilde{f}_1(\alpha')\tilde{f}_2(\alpha')\alpha' d\alpha' \tag{38}$$

Substituting (37) in (35) and taking the inner product of the resulting equations with each of the basis functions and finally employing Parseval's relation in HTD together with mixed boundary conditions, $E_{(\pm)}(\rho < a) = 0$ and $K_{(\pm)}(\rho > a) = 0$, at $z = d$ surface, we have:

$$\begin{bmatrix} Z_{im}^{++} & Z_{im}^{+-} \\ Z_{im}^{-+} & Z_{im}^{--} \end{bmatrix} \begin{bmatrix} C_{m(+)} \\ C_{m(-)} \end{bmatrix} = 0 \tag{39}$$

where

$$Z_{im}^{\pm\pm}(\omega) = \int_0^\infty \tilde{K}_{si(\pm)}(\alpha)Z_{\pm\pm}(\alpha,\omega)\tilde{K}_{sm(\pm)}(\alpha)\alpha d\alpha \tag{40}$$

$$Z_{im}^{+-}(\omega) = Z_{im}^{-+}(\omega) = \int_0^\infty \tilde{K}_{si(+)}(\alpha)Z_{+-}(\alpha,\omega)\tilde{K}_{sm(-)}(\alpha)\alpha d\alpha \tag{41}$$

Equation (39) has nontrivial solutions if the determinant of the coefficients matrix vanishes:

$$\det[Z_{im}] = 0 \tag{42}$$

This is the eigenvalue equation of the structure. In general, the roots of (42) are complex numbers. Let $\omega = 2\pi(f_r + jf_i)$, then the real and imaginary parts of the complex root is the resonant frequency and the damping factor of the structure, respectively. The quality factor of the structure which has an inverse proportion with its bandwidth is attained as $Q = f_r/2f_i$ [9].

## 4. RADIATION PATTERN

It is known [24, 25] that the Fourier transform of the aperture field gives the far-zone pattern. This quantity is defined as

$$\mathbf{F}_{x,y}(\alpha, \beta) = \frac{1}{\lambda^2} \int_{-\infty}^{\infty} \int_{-\infty}^{\infty} \mathbf{E}_a(x, y) e^{jk(\alpha x + \beta y)} dx dy \tag{43}$$

where $\alpha = \sin\theta\cos\phi$, $\beta = \sin\theta\sin\phi$ and $\gamma = \cos\theta$ are directional cosines.

For structure with circular symmetry, we can write (43) in polar coordination as

$$\mathbf{F}_{x,y}(\alpha, \beta) = \frac{1}{\lambda^2} \int_{-\infty}^{\infty} \int_{0}^{2\pi} \mathbf{E}_a(\rho) e^{jn\psi} e^{jk\rho\sin\theta\cos(\psi-\phi)} \rho d\psi d\rho \tag{44}$$

Using the Bessel function property of

$$J_n(x) = \frac{j^{-n}}{2\pi} \int_{0}^{2\pi} e^{jx\cos\phi} e^{jn\phi} \tag{45}$$

we get

$$\mathbf{F}_{x,y}(\alpha, \beta) = \frac{2\pi j^n}{\lambda^2} e^{jn\phi} \tilde{\mathbf{E}}_a(k\sin\theta) \tag{46}$$

The field components can be expressed in terms of $E_{(+)}$ and $E_{(-)}$ in (26) evaluated at $z = d$:

$$E_{ax} = E_{a\rho}\cos\phi - E_{a\phi}\sin\phi = \frac{1}{2}\left[E_{(+)}e^{j\phi} + E_{(-)}e^{-j\phi}\right] \tag{47}$$

$$E_{ay} = E_{a\rho}\sin\phi + E_{a\phi}\cos\phi = \frac{1}{2j}\left[E_{(+)}e^{j\phi} - E_{(-)}e^{-j\phi}\right] \tag{48}$$

Applying a saddle point method and after some mathematical manipulation, we have

$$E_\theta \stackrel{R\to\infty}{\sim} -k_0\frac{e^{-jkR}}{kR}j^n e^{jn\phi}\left[\tilde{E}_{(+)}(k_0\sin\theta) - \tilde{E}_{(-)}(k_0\sin\theta)\right] \tag{49}$$

$$E_\phi \stackrel{R\to\infty}{\sim} k_0\frac{e^{-jkR}}{kR}j^{n+1} e^{jn\phi}\left[\tilde{E}_{(+)}(k_0\sin\theta) - \tilde{E}_{(-)}(k_0\sin\theta)\right] \tag{50}$$

## 5. NUMERICAL RESULTS

In order to determine the resonant frequency and damping factor of the structure, the Galerkin's method is applied to (39). The basis functions are chosen to comply with the patch current solution of the structure using the wave equation on a cylindrical cavity [10] with magnetic wall boundary conditions, which for circular disc is

$$\frac{\partial E}{\partial \rho} \mid_{\rho=a} = 0 \tag{51}$$

The electric field expressions, for the circular disc structure is

$$E_z = E_0 J_n(k\rho) e^{jn\phi} \tag{52}$$

Since $\mathbf{E} = \hat{\mathbf{z}} E_z$, the magnetic fields components are

$$H_\rho = \frac{j}{\omega\mu} \frac{1}{\rho} \frac{\partial E_z}{\partial \phi} = -\frac{n}{\omega\mu\rho} E_0 J_n(k\rho) e^{jn\phi} \tag{53}$$

$$H_\phi = \frac{j}{\omega\mu} \frac{\partial E_z}{\partial \rho} = -\frac{j}{\omega\mu} E_0 \frac{\partial}{\partial \rho} \left[ J_n(k\rho) \right] e^{jn\phi} \tag{54}$$

The surface currents on the circular patch can be obtained from

$$\mathbf{K} = \hat{\mathbf{n}} \times \mathbf{H} = \hat{\mathbf{a}}_z \times (H_\rho \hat{\mathbf{a}}_\rho + H_\phi \hat{\mathbf{a}}_\phi) = \hat{\mathbf{a}}_\rho H_\phi - \hat{\mathbf{a}}_\phi H_\rho \tag{55}$$

At the edge of the disk, the radial component of the surface current, $\mathbf{K}$, must vanish; therefore

$$J_n'(ka) = 0 \tag{56}$$

Finally, the basis function is found by applying the same procedure as (25) to the tangential currents:

$$K_{sm(\pm)}(\rho) = H_{m\phi} \mp jH_{m\rho} = J_{n\pm1}(k_m\rho) \tag{57}$$

where

$$J_n'(k_m a) = 0 \tag{58}$$

Using the same procedure, the basis functions for annular ring structure are found as

$$K_{sm(\pm)}(\rho) = J_{n\pm1}(k_m\rho) - \frac{J_n'(k_m a)}{Y_n'(k_m a)} Y_{n\pm1}(k_m\rho) \tag{59}$$

and $k_m$ is the root of

$$J_n'(k_m b)Y_n'(k_m a) - J_n'(k_m a)Y_n'(k_m b) = 0 \tag{60}$$

where $J_n(x)$ is Bessel function of the first kind, $Y_n(x)$ is Bessel function of the second kind and the primes denote the first derivative with respect to the argument.

These basis functions can fortunately be analytically Hankel transformed. Simpson method is employed to carry out numerical integrations for matrix elements in (40), (41) and Muller method is used for root finding of (42). In order to consider the effects of the fringing fields around the patch, the effective radius is considered as in [26]. For any values of patch radius, substrate thickness and dielectric permittivity, only few computer seconds are needed to determine the resonant frequency and the quality factor.

Tables 1 and 2 compare the experimental results reported in [11] and [17] respectively for circular disk and annular ring microstrip antenna with the numerical method presented in this paper. These comparisons indicate excellent agreements for isotropic substrate case. In Fig. 2, a comparison is done for radiation pattern of circular disk microstrip antenna between experimental results reported in [11] and our results which have excellent agreement either.

Next, the effect of uniaxial anisotropy on the resonant frequency, quality factor and radiation pattern of the structure is analyzed. The
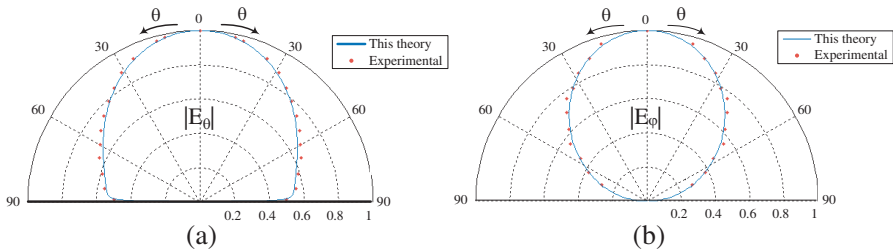


**Figure 2.** Radiation pattern of the fundamental resonant mode of a circular disk microstrip antenna on a single dielectric substrate ($\varepsilon_{r1}$, $d = 1.5875\,\text{mm}$, $d/a = 0.0236$). (a) $E_\theta$. (b) $E_\phi$.

**Table 1.** Comparison of the experimental results in [11] with the results of the numerical method of this paper for the resonant frequency of the fundamental mode of a circular microstrip patch on a single layer isotropic dielectric substrate of permittivity $\varepsilon_r = 2.43$ and thickness $d = 0.49\,\text{mm}$.

| $a/d$ | $f_r$ (Numerical) (GHz) | $f_r$ (Experimental) (GHz) | Error% |
|-------|-------------------------|----------------------------|--------|
| 4.02 | 25.4 | 25.3 | $-0.4$ |
| 8.08 | 13.3 | 13.1 | $-1.5$ |
| 12.02 | 9.2 | 9.0 | $-2.6$ |
| 20.33 | 5.6 | 5.5 | $-2.3$ |

**Table 2.** Comparison of the experimental results in [17] with the results of the numerical method of this paper for the resonant frequency of the fundamental mode of an annular ring microstrip patch on a single layer isotropic dielectric substrate of permittivity $\varepsilon_r = 2.32$ and thickness $d = 0.49$ mm. The ratio of the outer and inner radius of the ring is $b/a = 2$.

| $a$ (mm) | $f_r$ (Numerical) (GHz) | $f_r$ (Experimental) (GHz) | Error% |
|---|---|---|---|
| 25 | 0.894 | 0.876 | −2.06 |
| 35 | 0.642 | 0.626 | −2.72 |
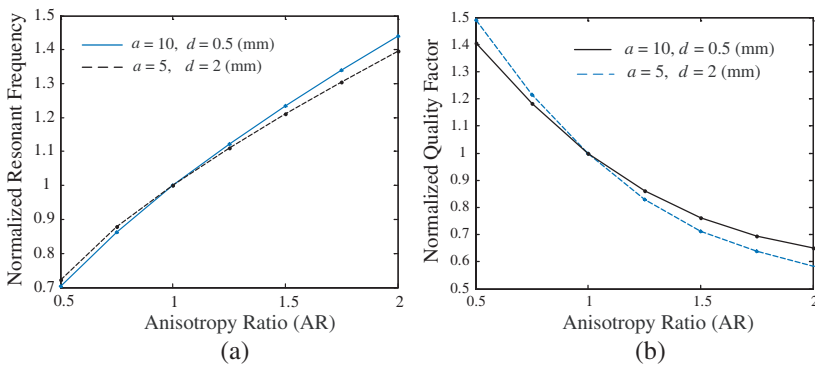


**Figure 3.** (a) Normalized resonant frequency. (b) Normalized quality factor of circular patch microstrip antenna versus anisotrpy ratio when $\varepsilon_{r2} = 2.43 \ \varepsilon_{r1}$ varies.

anisotropy ratio $(AR)$ is defined as $AR = \varepsilon_2/\varepsilon_1$. Fig. 3(a) represents the normalized resonant frequency of the fundamental mode versus anisotropy ratio for a circular patch printed on a uniaxial substrate at different values of patch radius and substrate thickness. As anisotropy ratio changes from 0.5 to 2, the normalized resonant frequency varies by approximately 0.7. Thus, considering the narrow bandwidth of microstrip antennas, the anisotropy effect on the resonant frequency can not be ignored and must be taken into account in the design procedure. In addition, the resonant frequency reduction could be used for reducing the radiating element size or attending desired directivity as shown later.

In Fig. 3(b) the variation of antenna quality factor with respect to anisotropy ratio is shown. It is observed that in order to decrease the quality factor to achieve wider bandwidths, anisotropy ratio must be more than unity. Using an anisotropy ratio less than one leads to a high quality factor suitable for resonator design.

In Fig. 4 the author compares the radiation patterns obtained for two circular disk microstrip antennas on uniaxial substrates with two different values of anisotropy ratio of 0.75 and 1.75. It is observed that the directivity of the antenna with greater value of anisotropy ratio is more than the smaller one. This treatment has physical agreement with the results obtained in Fig. 3(a). We saw in Fig. 3(a) that the greater anisotropy ratio the greater resonant frequency and of course the smaller operating wavelength. Concerning that the patch size is frozen, the ratio of patch size to wavelength will be greater and accordingly we get greater directivity.

Similar results are achieved for annular ring microstrip antenna in Fig. 5(a), Fig. 5(b) and Fig. 6 for resonant frequency, quality factor and radiation patterns respectively.
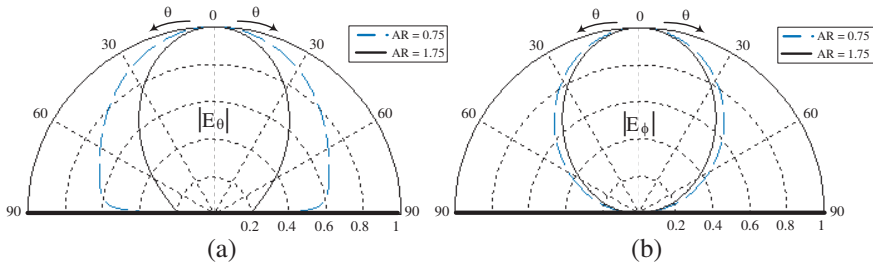


**Figure 4.** Radiation patterns of the fundamental resonant mode of a circular disk microstrip antenna on uniaxial substrate for two different values of anisotropy ratio. $\varepsilon_{r2} = 2.43$, $d = 1\,\text{mm}$, $a = 10\,\text{mm}$. (a) $E_\theta$. (b) $E_\phi$.
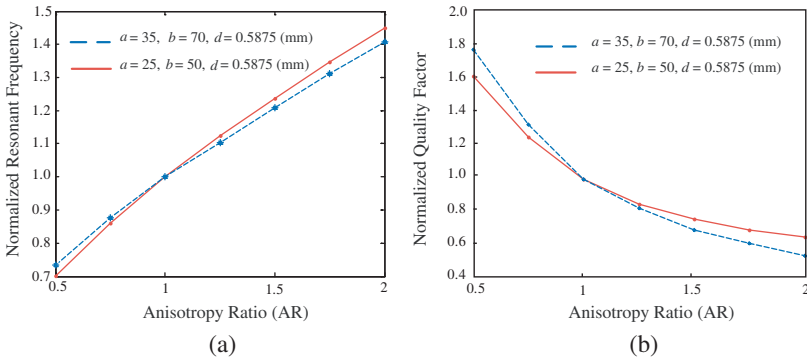


**Figure 5.** (a) Normalized resonant frequency. (b) Normalized quality factor of annular ring microstrip antenna versus anisotrpy ratio when $\varepsilon_{r2} = 2.32$ and $\varepsilon_{r1}$ varies.
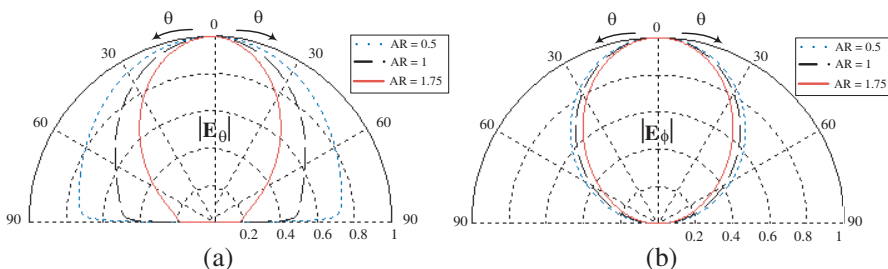
**Figure 6.** Radiation patterns of the fundamental resonant mode of an anular ring microstrip antenna on uniaxial substartes for two different values of anisotropy ratio. $\varepsilon_{r2} = 2.32$, $d = 1.5875\,\text{mm}$, $a = 25\,\text{mm}$, $b = 50\,\text{mm}$. (a) $E_\theta$. (b) $E_\phi$.

## 6. CONCLUSION

An analytical solution of a circular disk and annular ring microstrip antenna with uniaxial anisotropic substrate is derived in Hankel transform domain using Hertz potential vectors. The analytical solution not only gives a better understanding of the physical problem, but also provides an accurate and fast method to find the resonant and far field characteristics of the structures. Galerkin's method together with parsval's relation in Hankel transform domain has been used for the numerical calculation of resonant frequency and quality factor of the first resonant modes of circular disk and annular ring patches. Finally, radiation pattern of the structures are found using the angular spectrum theorem. The results prove that there is considerable resonant frequency shift, quality factor value change and radiation pattern variations due to anisotropy of the substrate.

## REFERENCES

1. Alexopoulos, N. G., "Integrated circuit structures on anisotropic substrates," *IEEE Trans. Microwave Theory Tech.*, Vol. 33, 847–881, Oct. 1985.

2. Alexopoulos, N. G. and S. A. Maas, "Characteristics of microstrip directional couplers on anisotropic substrates," *IEEE Trans. Microwave Theory Tech.*, Vol. 30, 1267–1270, Aug. 1982.

3. Drake, E., R. R. Boix, M. Horno, and T. K. Sarkar, "Effect of substrate dielectric anisotropy on the frequency behavior of microstrip circuits," *IEEE Trans. Microwave Theory Tech.*, Vol. 30, 1267–1270, Aug. 1982.

4.  Yang, H. Y. and N. G. Alexopoulos, "Uniaxial and biaxial substrate effects on finline characteristics," *IEEE Trans. Microwave Theory Tech.*, Vol. 35, 24–29, Jan. 1987.

5.  Bouttout, F., F. Benabdelaziz, A. Benghalia, D. Khedrouche, and T. Fortaki, "Uniaxially anisotropic substrate effects on resonance of rectangular microstrip patch antenna," *Electron. Lett.*, Vol. 35, No. 4, 255–256, Feb. 1999.

6.  Zhao, A., J. Juntunen, and A. V. Risnen, "An efficient FDTD algorithm for the analysis of microstrip patch antennas printed on a general anisotropic dielectric substrate," *IEEE Trans. Microwave Theory Tech.*, Vol. 47, No. 7, Jul. 1999.

7.  Pozar, D. M., "Radiation and scattering from a micro strip patch on a uniaxial substrate," *IEEE Trans. Antennas Propagat.*, Vol. 35, 613–621, Jun. 1987.

8.  Campos, A. L. P. S. and A. G. D'Assunqiio, "Hertz vector potential analysis of FSS on anisotropic substrates," *Proceedings SBMO/IEEE MTT-S IMOC*, 2003.

9.  Michalski, K. A. and D. Zheng, "Analysis of microstrip resonators of arbitrary shape," *IEEE Trans. Microwave Theory Tech.*, Vol. 40, 112–119, Jan. 1992.

10. Bahl, I. J. and P. Bhartia, *Mirostrip Antennas*, Artech House, 1980.

11. Losada, V., R. R. Boix, and M. Horn, "Resonant modes of circular microstrip patches in multilayered substrate," *IEEE Trans. Antennas propagat.*, Vol. 47, No. 4, Apr. 1999.

12. Losada, V., R. R. Boix, and M. Horno, "Full wave analysis of circular microstrip resonators in multilayered media containing uniaxial anisotropic dielectrics, magnetized ferrites, and chiral materials," *IEEE Trans. Microwave Theory Tech.*, Vol. 48, 1057–1064, Jun. 2000.

13. Curel, C. S. and E. Yazgan, "Characteristics of a circular patch microstrip antenna on uniaxialiy anisotropic substrate," *IEEE Trans. Antennas Propagat.*, Vol. 52, No. 10, Oct. 2003.

14. Losada, V., R. R. Boix, and F. Medina, "Resonant modes of stacked circular microstrip patches in multilayered substrates containing anisotropic and chiral materials," *Journal of Electromagnetic Waves and Applications*, Vol. 17, No. 4, 619–640, 2003.

15. Row, J.-S., "Dual-frequency circularly polarised annular-ring microstrip antenna," *Electron. Lett.*, Vol. 40, No. 3, Feb. 2004.

16. Bahl, I. J., S. Stuchly, and M. A. Stuchly, "A new microstrip radiator for medical applications," *IEEE Trans. Microwave*

*Theory Tech.*, Vol. 28, No. 12, Dec. 1980.

17. Gomez-Tagle, J. and C. G. Christodoulou, "Extended cavity model analysis of stacked microstrip ring antenna," *IEEE Trans. Antennas Propagat.*, Vol. 45, No. 11, Nov. 1997.

18. Ali, S. M., W. C. Chew, and J. A. Kong, "Vector hankel transform analysis of annular-ring microstrip antenna," *IEEE Trans. Antennas Propagat.*, Vol. 30, 637–644, Jul. 1982.

19. Wu, Y. S. and F. J. Rosenbaum, " Mode chart for microstrip ring resonators," *IEEE Trans. Microwave Theory Tech.*, Jul. 1973.

20. Barkat, Q and A. Benghalia, "Radiation and resonant frequency of superconducting annular ring microstrip antenna on uniaxial anisotropic media," *Journal of Infrared, Millimeter and Terahertz*, Vol. 30, No. 10, 1053–1066, Jun. 2009.

21. Gurel, G. S. and E. Yazgan, "Resonance in microstrip ring resonator with uniaxially anisotropic substrate and superstrate layers," *Journal of Electromagnetic Waves and Applications*, Vol. 4, No. 8–9, 1135–1144, 2010.

22. Silva. S. G., J. R. S. Oliveira., and A. G. Dassuno, "Annular ring microstrip antennas for millimeter wave applications," *Int. Journal of Infrared and Millimeter Waves*, 821–829, Apr. 2007.

23. Collin, R. E., *Field Theory of Guided Waves*, 2nd edition, IEEE Press, New York, 1991.

24. Araki, K. and T. Itoh, "Hankel transform domain analysis of open circular microstrip radiating structure," *IEEE Trans. Antennas Propagat.*, Vol. 29, No. 1, Jan. 1981.

25. Clarke, R. H., *Diffraction Theory and Antenna*, Wiley, New York, 1980.

26. Balanis, C. A., *Antenna Theory-Analysis and Design*, 3rd edition, Wiley, New York, 2005.